ARTICLE

Marlim R3D: a realistic model for CSEM simulations — phase I: model building

Marlim R3D: um modelo realista para simulações CSEM — fase 1: construção do modelo

Bruno Rodrigues Carvalho[1], Paulo Tarso Luiz Menezes[1]*

ABSTRACT: The marine controlled-source electromagnetic (CSEM) method provides complementary information to seismic imaging in the exploration of sedimentary basins. The CSEM is mainly used for reservoir scanning and appraisal. The CSEM interpretation workflow is heavily based on inversion and forward — modeling for hypothesis testing. Until the recent past, the effectiveness of a given workflow was achieved after the drilling results, as there wasn't any geological complex model available to serve as a benchmark. In the present paper, we describe the workflow to build up Marlim R3D, a realistic and complex geoelectric model. Marlim R3D aims to be a reference model of turbidite reservoirs of the Brazilian continental margin. Our model is based on seismic interpretation and constrained by the input of available well-log information. The workflow used is composed of seven steps: seismic and well-log dataset loading, well-tie, *Vp* cube construction, *Vp* resistivity calibration, time-depth conversion, resistivity cube construction, and quality-control check. As a result, we obtained an interpreted dataset composed by main stratigraphic horizons, pseudo-well logs, and the resistivity cubes. These elements were made freely available for research or commercial use, under the Creative Common License, at the Zenodo platform.

KEYWORDS: turbidites; CSEM; reservoir model.

RESUMO: *O método eletromagnético marinho de fonte controlada (CSEM) fornece informações complementares à imagem sísmica na exploração de bacias sedimentares. O CSEM é usado principalmente para escaneamento e avaliação de reservatórios. O fluxo de trabalho de interpretação CSEM é fortemente baseado em inversão e modelagem direta para testes de hipóteses. Até o passado recente, a efetividade de determinado fluxo de trabalho era alcançada somente após os resultados de perfuração. Isso em virtude de não haver nenhum modelo geológico complexo disponível para servir de referência. No presente trabalho, descrevemos o fluxo de trabalho para construir o Marlim R3D, um modelo geoelétrico realista e complexo. Marlim R3D pretende ser um modelo de referência de reservatórios de turbiditos da margem continental brasileira. Nosso modelo baseia-se na interpretação sísmica calibrada por perfis de poços disponíveis. O fluxo de trabalho empregado é composto de sete etapas: carregamento de dados sísmicos e de perfis de poços, amarração sísmica-poço, construção de cubo Vp, calibração de Vp resistividade, conversão tempo-profundidade, construção de cubo de resistividade e controle de qualidade. Os elementos obtidos na construção de Marlim R3D (cubos, horizontes e perfis de resistividade em poços) são disponibilizados gratuitamente para pesquisa ou uso comercial, sob a Licença Creative Common, na plataforma Zenodo.*

PALAVRAS-CHAVE: *turbiditos; CSEM; modelo de reservatório.*

INTRODUCTION

The marine controlled-source electromagnetic (CSEM) method has been accepted as a risk reduction tool in the petroleum industry. In its most typical survey configuration, it uses a horizontal electric dipole source transmitting, towed close to the marine substrate, a low-frequency (0.01 to 3 Hz) electromagnetic signal. The receivers are sensors that, deposited on the ocean floor, can measure up to three components (X, Y, Z). More details on the method's theory can be obtained in Edwards (2005) and Constable and

Srnka (2007). The CSEM method had its initial development around the 1970 decade, aimed at solving academic studies in the mapping of the resistivity structure of the marine floor at great depths (Constable & Cox 1996).

The success of these pioneering experiments enabled the expansion of CSEM usage in the 1980s and 1990s, with the unveiling of the geoelectric structure of mid-ocean ridges and submarine magmatic systems (Evans *et al.* 1994).

The application of CSEM in the oil industry began in the 2000s, with the pioneering survey in deep waters of Angola, and reached a market scale in the year of 2004 (Constable

& Srnka 2007). In 2007, the first reduction in the business activities happened. MacGregor and Tomlinson (2014) point out the lack of reliable interpretation workflows as one of the possible causes of this downfall. At that time, the effectiveness and accuracy of a given workflow were only available after *post-mortem* analysis of the well result.

Data generated by synthetic geoelectric models can be used to evaluate a CSEM workflow effectiveness. Most of the available models are simple physical models with a known mathematical formulation. These models are suitable for software development, but they are inefficient to represent the geological complexity of the marine substrate adequately and, hence, tend to negatively impact the workflow of real data interpretation in the hydrocarbon exploration industry (Tseng *et al.* 2015).

The Society of Exploration Geophysicists (SEG) recognized that issue and developed a special project for the construction of a multi-physics model, the so-called SEG Advanced Modeling (SEAM) (Fehler 2009). The SEAM Phase 1 model was constructed to represent the complex geology of the region of the allochthonous salt domains deep waters of the Gulf of Mexico (United States).

The SEAM-1 model occupies a rectangular area of approximately 1,400 km2. It measures 35 km in the east-west direction, 40 km in the north-south and reaches 15 km in depth. Also, it is complex enough to realistically represent faults and other geological features associated with the presence of allochthonous salt bodies, such as overturned beds and overhanging salt. In the salt bodies, some turbiditic fans and braided stream channels were modeled as the hydrocarbon reservoirs in the region.

The SEAM-1 is a multi-physics model that includes 3D cubes of compressional velocity (Vp), shear velocity (Vs), density (ρ), horizontal (ρh) and vertical (ρv) resistivities. Thus, it can be used for seismic, gravimetric and electromagnetic stand-alone or joint simulations. Since its implementation, SEAM-1 has been used by the oil companies in-house simulations, and also in the academy (Tseng *et al.* 2015).

In the Brazilian continental margin, turbiditic bodies make up the main post-salt plays and possible targets for CSEM surveys. Those types of reservoirs are not portrayed in the SEAM-1 models. To fill this gap, we have developed the Marlim R3D (MR3D), a realistic anisotropic geoelectric model that aims to be a standard for CSEM studies of the turbiditic reservoirs of the Brazilian continental margin (Fig, 1). Our model includes fine-scale stratigraphy and fluid-filled reservoirs, and measures 27 km north-south by 24 km east-west by 6 km depth.

MR3D is based on previous 3D seismic interpretation (Nascimento *et al.* 2014) and constrained by public well-log data and regional geological information.

In the present paper, we concentrate on the description of the geoelectric model building at a seven sequential steps workflow: seismic and well-log database, well-tie, Vp cube, Vp resistivity calibration, time-depth conversion, resistivity cube output, and quality-control check.

The interpreted dataset including 3D cubes of (ρh) and (ρv) resistivities in SEG-Y format, composed by main stratigraphic horizons, pseudo- well-ogs, are freely downloadable, for research or commercial use, under the Creative Common License, on the Zenodo (Carvalho & Menezes, 2017).

CAMPOS BASIN STRATIGRAPHIC SETTING

The sedimentary section of the Campos Basin can be grouped into three mega-sequences associated to the following tectonic development stages: rift, transitional and drift (Fig. 2).

The Barremian lacustrine sediments of Lagoa Feia Formation overlie the Hauterivian Cabiu´nas basalts (120–130 Ma); these basalts represent the economic basement of Campos Basin. The Lagoa Feia sediments are recognized as the most valuable source rocks in the Campos Basin.

The Aptian sequence contains, from base to top: conglomerates, carbonates and evaporitic rocks deposited during a period of tectonic quiescence. This transitional stage expresses the beginning of the drift phase in which the sediments are correlated with the first sea-water inflows through the Walvis Ridge (Leyden *et al.* 1976).

The drift stage commences with a marine mega-sequence characterized by the Albian/Cenomanian shallow-water calcarenites and calcilutites of Maca´e Formation. The marine Upper Cretaceous to Paleogene deep-water clastic section (Carapebus Formation) is composed of shale, marls and sandstone turbidites, deposited in a period of general tectonic quiescence and of continued subsidence. The turbidite systems constitute the most valuable petroleum reservoirs in the Campos Basin (Bruhn *et al.* 2003). Progradational siliciclastic sequences characterize the Neogene section. In the deep-water of the Campos Basin, the deposition of this mega-sequence was greatly conditioned by salt tectonics (Mohriak *et al.* 1996).

MODEL BUILDING WORKFLOW

There are several options for building a 3D geoelectric model. Park *et al.* (2015), for example, interpolate and extrapolate the resistivities of wells respecting the stratigraphy along the studied area. However, for the application

of such technique, it is necessary to have a large number of wells in hand, and that these wells should have information of the entire stratigraphic column to be extrapolated. A relative weakness of that approach is the fact that lateral facies variation between the wells cannot be adequately represented through the simple interpolation.

A second widely used alternative is the construction of the resistivity cube based on a velocity—porosity—resistivity petrophysical models available in the literature (Hashin & Shtrikman 1962; Hermance 1979; Werthmu̇ller *et al.* 2013).

In the present work, we estimate the direct relationship between velocity and resistivity, then we use this relation to interpolate and extrapolate the resistivities accompanying previous stratigraphic knowledge throughout the study area. To this end, we defined a workflow consisting of seven main stages:

- Seismic and well-log database;
- Seismic-well tie;
- *Vp* cube;
- *Vp* x resistivity relationship;
- Time to depth conversion;
- Resistivity cubes;
- Quality control.

Seismic and well-log database

In late 1996, early 1997, Geco-Prakla collected for Petrobras the 3D seismic data interpreted in this study. The survey area spanned over 720 km (Johann *et al.*, 2009). The survey acquisition parameters are presented in Table 1.
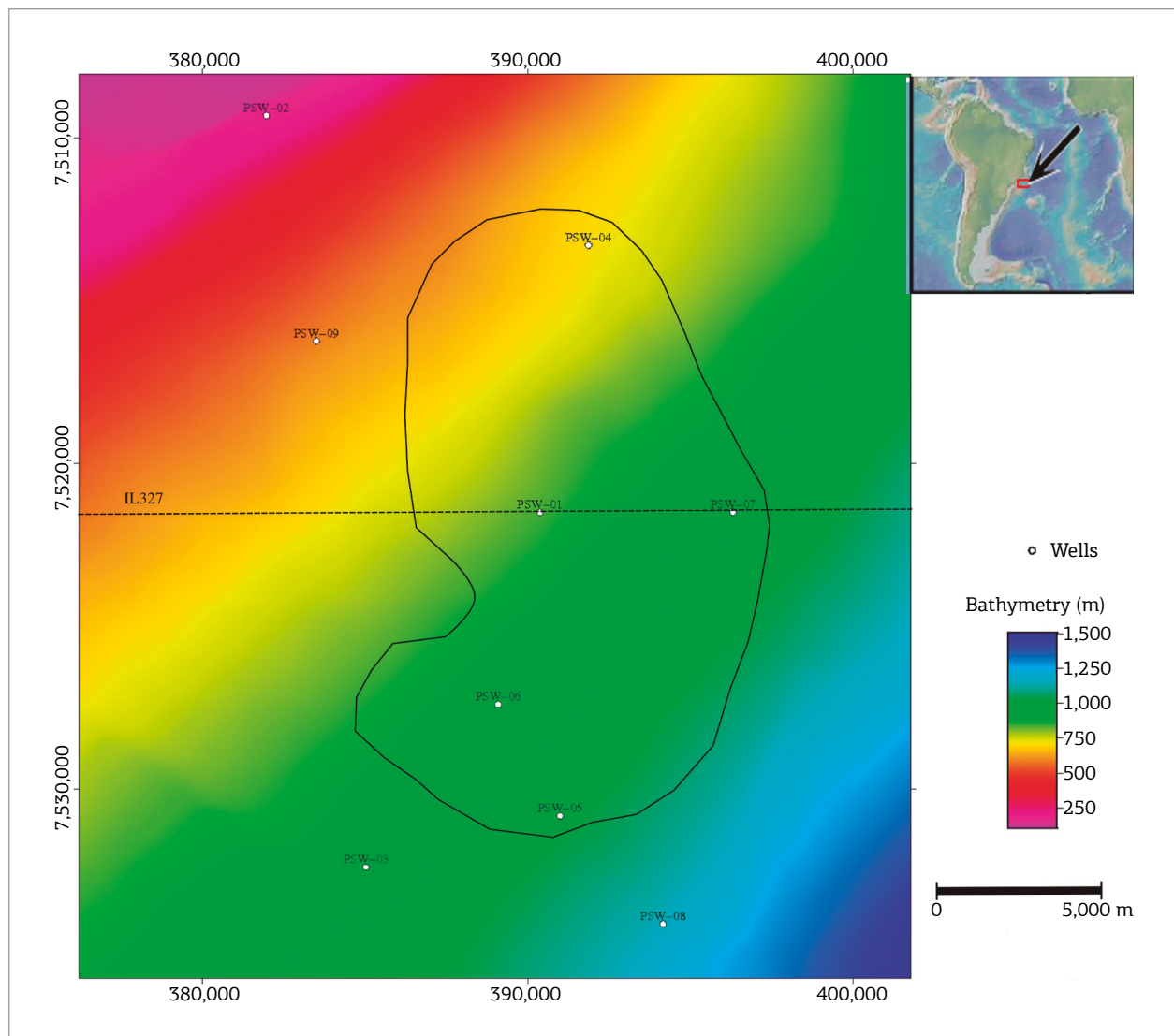

Figure 1. Location map of the seismic dataset at Marlim field. Coordinates are in UTM, zone 39S. Marlim reservoir outline is shown in the black line. The dashed lines corresponds to the interpreted inline 327. PSW-01 to PSW-09 are the available wells.

The Brazilian Petroleum Agency (ANP) made available the public seismic dataset by providing a post-stack time-migrated 3D seismic amplitude cube (Tab. 2), as well as check shots, stratigraphic markers, and composite well logs — density (ρ), sonic (DT), porosity (φ), gamma ray (GR), and horizontal resistivity (ρh) of nine wells in the study area (Fig. 1).

We have built an integrated database in an open-source seismic platform and loaded the wells' information (stratigraphic markers and well-log curves), the dip-steering (DS) filtered seismic data and the main stratigraphic horizons interpreted by Nascimento *et al.* (2014). Those authors have shown that the DS filtered data, in which random spurious noises were attenuated, highlight the main reflections related to stratigraphy and therefore they would be more amenable to interpretation.

The high quality of the filtered seismic data and the six main stratigraphic horizons from the seafloor to the bottom of the salt, according to theinterpretation, are illustrated in Figure 3.

Well-log editing

We have applied an editing and preconditioning filtering step for the well data. All log curves were cascade filtered

with a spike removal filter followed by a low-pass moving average filter. That step is necessary to remove undesirable

Table 1. Seismic acquisition parameters.

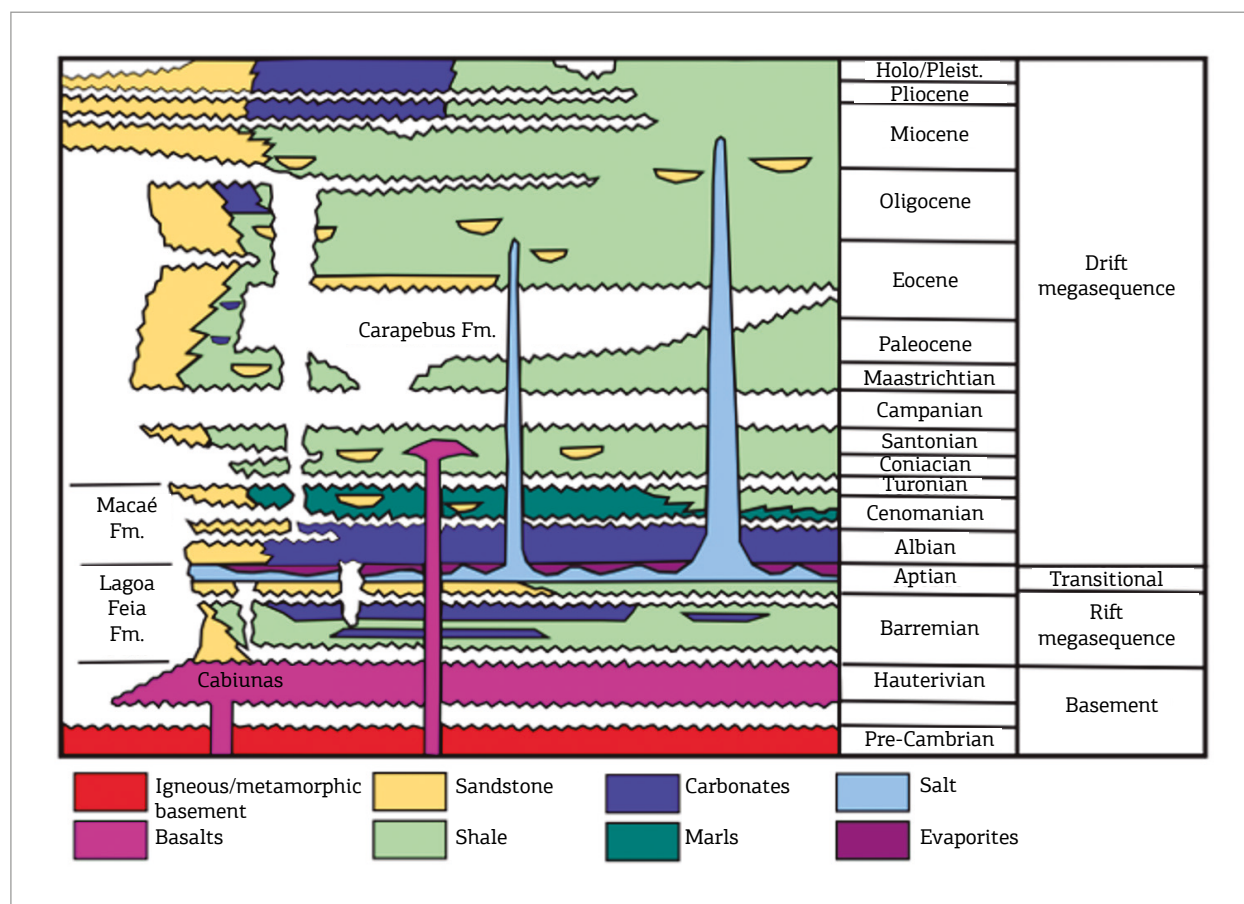|	1997 Acquisition
Area (km2)	720
Number of cables	6
Spreads (offset, m)	0-148-3535.5
Channels/cable	288
Shot point interval (m)	25
Receiver interval (m)	12.5
Cable interval (m)	50
Sample rate (ms)	1
Bin size (m)	12.5 × 25
Cable depth (m)	9
Azimuth (degrees)	123
Nominal fold	72
Traces/km²	230,400

Figure 2. Simplified stratigraphic chart of the Campos Basin, modified from Guardado *et al.* (2000).

noise, and to bring the log information closer to the seismic resolution.

We calculated the Vp logs from the sonic curves by using the $Vp = 1/DT$ relation. Sequentially, we computed the acoustic impedance (AI) logs from (Vp) and density logs.

Seismic-well tie

Well ties are an essential part of the interpreter's job. The major goal is to correlate the stratigraphic markers described in the wells with the seismic reflections aiming to provide a correct identification of the horizons to pick. Getting a well tie is quite simple: synthetic seismograms calculated from well-log curves are matched to the actual seismic traces, and the features of the well in the depth domain are correlated to the seismic data in the time domain.

Synthetic seismograms are obtained from the convolution of the reflectivity series in time with a wavelet representing the seismic source. Frequently interpreters extract that wavelet from the seismic data (White & Simm 2003).

The acoustic impedance (AI) and the reflectivity (Rp) for any two given media are defined, respectively, by Equations 1 and 2.

$$AI = Vp \times \rho, \tag{1}$$

$$Rp = \frac{AI_2 - AI_1}{AI_1 + AI_2}; \tag{2}$$

In which:
AI1 and AI2 correspond, respectively, to the impedance of the first and second layers.

In the present study, we performed the seismic-well tie process by employing the following steps:

Table 2. 3D cube parameters.

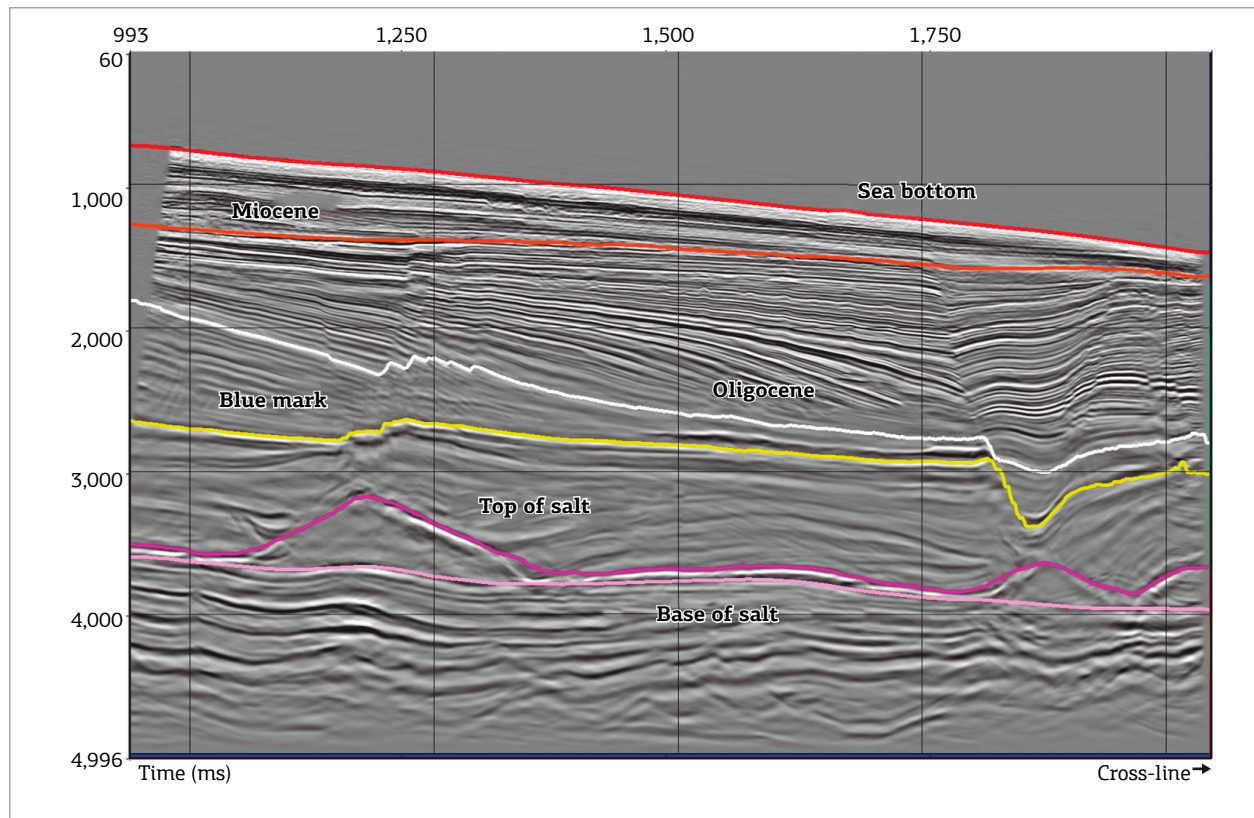| Parameter	Quantity
Inlines	429
Inlines direction	east–west
Inlines spacing	25 m
Crosslines	1,115
Crosslines direction	north–south
Crossline spacing	12,5 m
Time window	60–4,996 miliseconds
Sampling rate	4 miliseconds

Figure 3. Inline 327 with the main interpreted seismic horizons.

- The seismic traces are bounded by a time window (taper length) and then extracted;
- Autocorrelation, in the time domain, of the seismic traces within the window defined in the previous step;
- Employ the direct Fourier transform to obtain the auto-correlation's frequency spectrum;
- Calculate the square root of the frequency spectrum's module and then subtract the zero frequency component;
- Apply the inverse Fourier transform; the real part of the inverse of the Fourier transform corresponds to extracted zero phase wavelet in time.

The final step of the seismic-well tie is given by the association between the synthetic seismogram and the seismic data in the vicinity of the well, resulting in a correlation panel for each well, as shown in Figure 4.

Vp cube

The *Vp* cube was built from the interpolation of the *Vp* curves along the studied area. At depths beyond the wells' information, we employed *Vp* estimates available in the literature.

The interpolation follows the stratigraphic knowledge given by the interpreted horizons along a Horizon Cube by Groot *et al.* (2010), which consists of a dense 3D set of stratigraphic surfaces associated with a given geological age. Consequently, hundreds of chrono-stratigraphically

correlated horizons, with similar strike and dip, are generated (Qayyum & Smith 2014).

The Horizon Cube was created using six stratigraphic intervals, bounded by the main horizons mapped by Nascimento *et al.* (2014): Seabed–Miocene, Miocene–Oligocene, Oligocene–Blue Mark, Blue Mark–Top of Salt, Top of Salt–Base of Salt, and Base of Salt–End of Model. The latter one, a 4,976 m time-slice horizon, aiming to represent the base of the model.

The Horizon Cube is shown in Figure 5A, and the *Vp* cube is shown in Figure 5B. We used a single velocity of 4,500 m/s to the salt sequence (Schön 2015), and a regional velocity trend published by Bulhões *et al.* (2015) to the sediments of the Lagoa Feia Group up to the basement rocks.

Vp x resistivity relationship

Background resistivity

Relations between elastic and electrical rock properties have been investigated both theoretically (*e.g.*, Carcione *et al.* 2007) and empirically (*e.g.*, Faust 1953; Gomez *et al.* 2010). Primary applications of such cross-property relationship include filling in data gaps when one property is more readily available than the other. Advanced uses of such relationship include the input of a priori information to reduce ambiguity in the inversion process (Mukerji *et al.* 2009; Werthmüller *et al.* 2013).
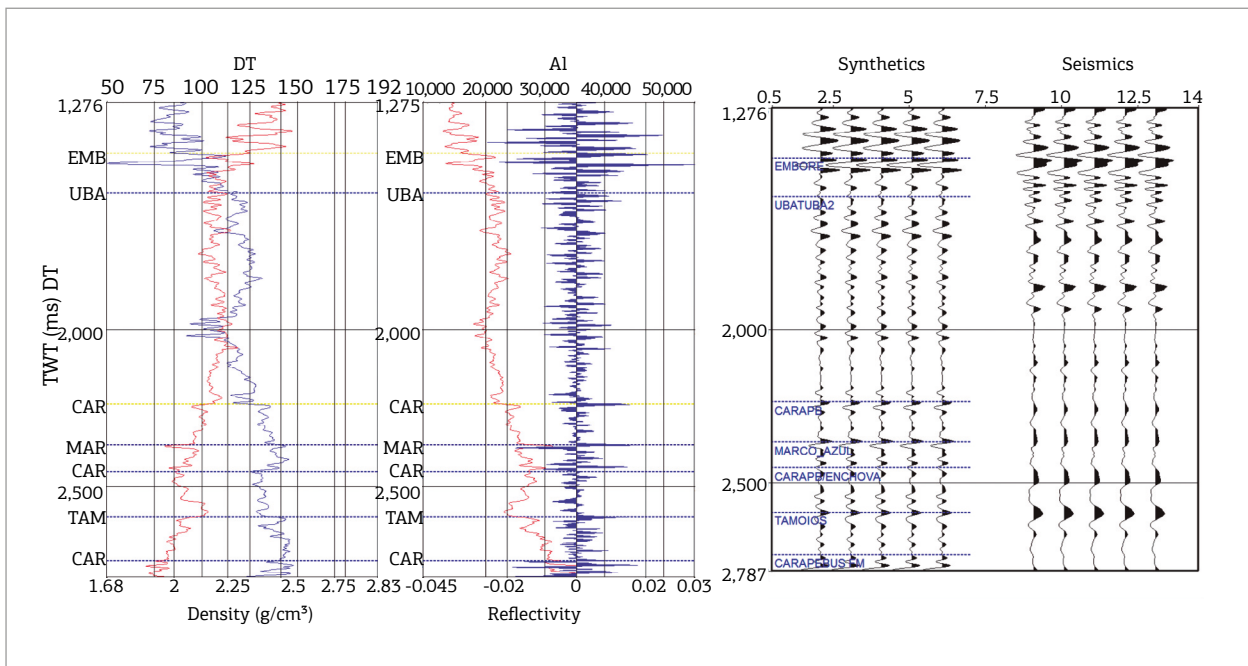

Figure 4. Well-tie correlation panel. Left panel) sonic (red curve) and density (blue curve) logs in the 1,276 to 2,797 ms time interval; central panel) acoustic impedance (AI) log (red curve) and reflectivity (blue curve). Right panel comparison between the synthetic and acquired seismic. EMB (Emboré), UBA (Ubatuba), CAR (Carapeba), MAR (Marco Azul), and TAM (Tamoios) are stratigraphic markers.

Faust (1953) has shown that both resistivity and velocity behave similarly with increasing depth. To investigate that subject in the studied area, we plotted in Figure 6 the measured horizontal resistivity (ρh) and Vp at all available wells against depth. As our goal was to define the background (or regional) resistivity, we did not take into
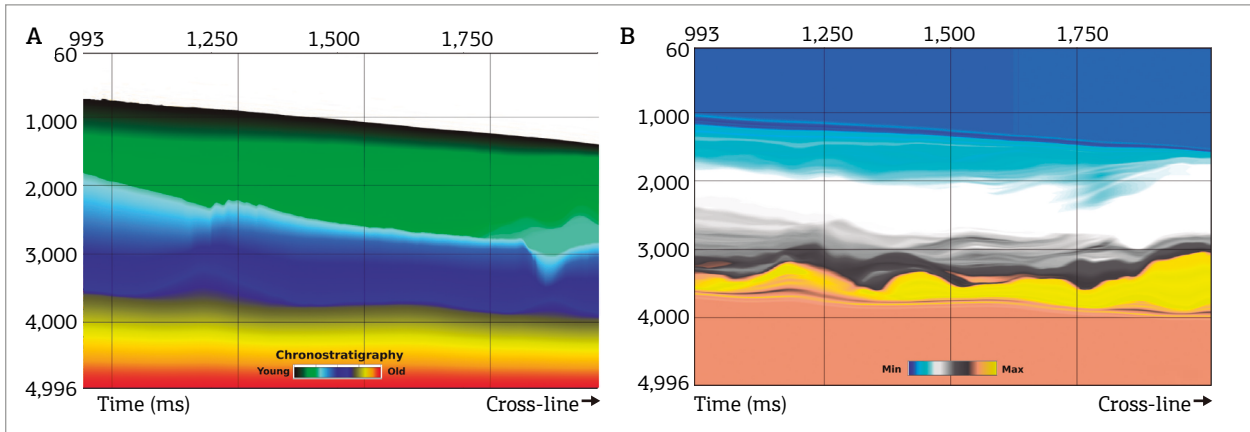

Figure 5. (A) Inline 327 extracted from the Horizon Cube, a stack of chronostratigraphic 3D horizons extracted at inline 317; (B) Vp interpolated along the inline 327 from the Horizon Cube shown in Figure 5A.
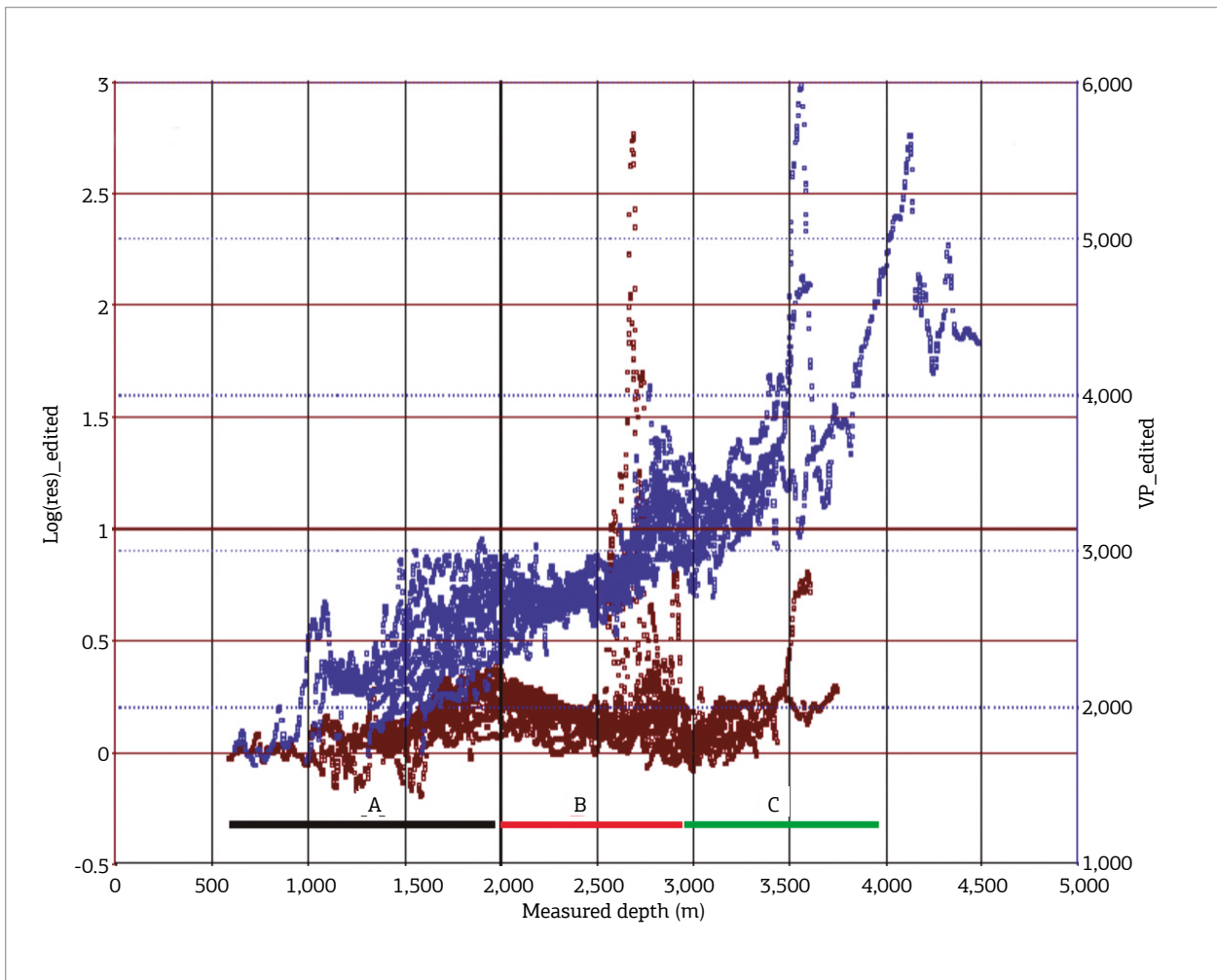

Figure 6. Vp (blue) and resistivity (brown) logs of all nine wells plotted *versus* depth. A, B, and C are depth intervals herein interpreted.

account the high resistivity values associated with the reservoir (average of 70o hm.m).

In Figure 6 we have classified three distinct zones: 600–2,000 m (zone A), 2,000–2,900 m (zone B), and depths greater than 2,900 m (zone C). Then, we calculated the relationship between log(ρh) and Vp by crossploting these two quantities at each identified A, B, and C depth zones. The crossplots of the respective zones are shown in Figures 7A, 7B and 7C. Hence, by least-squares fitting, we obtained three linear equations (Eqs. 3, 4 and 5) relating the background horizontal resistivity and velocity.

$$\rho h \; 600{-}2{,}000 \; m = -0.263 + 0.000166 \; Vp, \qquad (3)$$

$$\rho h \; 2{,}000{-}2{,}900 \; m = -0.0683 + 2{,}798.10\text{-}5 Vp, \qquad (4)$$

$$\rho h {>} 2{,}900 = -0.09 + 0.00037 Vp \qquad (5)$$

In which ρh 600–2,000 m, ρh 2,000–2,900 m, and ρh 2,900–end represent, respectively, the horizontal resistivity in the range of 1,000–2,000 meters, 2,000–2,900 meters and depths greater than 2,900 meters. At depth zone C,

the exception is the salt sequence (defined by top and base of salt horizons), where we assigned the single value of 1,000 ohm.m (Zerilli *et al.* 2016).

Anomalous resistivity

The high resistivities associated with the oil-prone Marlim turbidite sands match the anomalous reservoir values embedded in the low-resistivity regional background of the non-reservoir facies in depth zone b (Eq. 4).

Consequently, it is necessary to distinguish between the reservoir and the non-reservoir facies, and then associate the anomalous resistivity value only to the reservoir facies. To that end, we follow the interpretation of Nascimento *et al.* (2014), that described the reservoir facies with the acoustic impedance lower–equal than 5,700 *m/s.g/cm³* and porosity in the 0.26–0.32% range.

To that end, we created an algorithm (Algorithm 1) to identify and assign the Marlim reservoir facies resistivity and distinguish it from the background values. The input are the Vp, porosity and AI cubes.

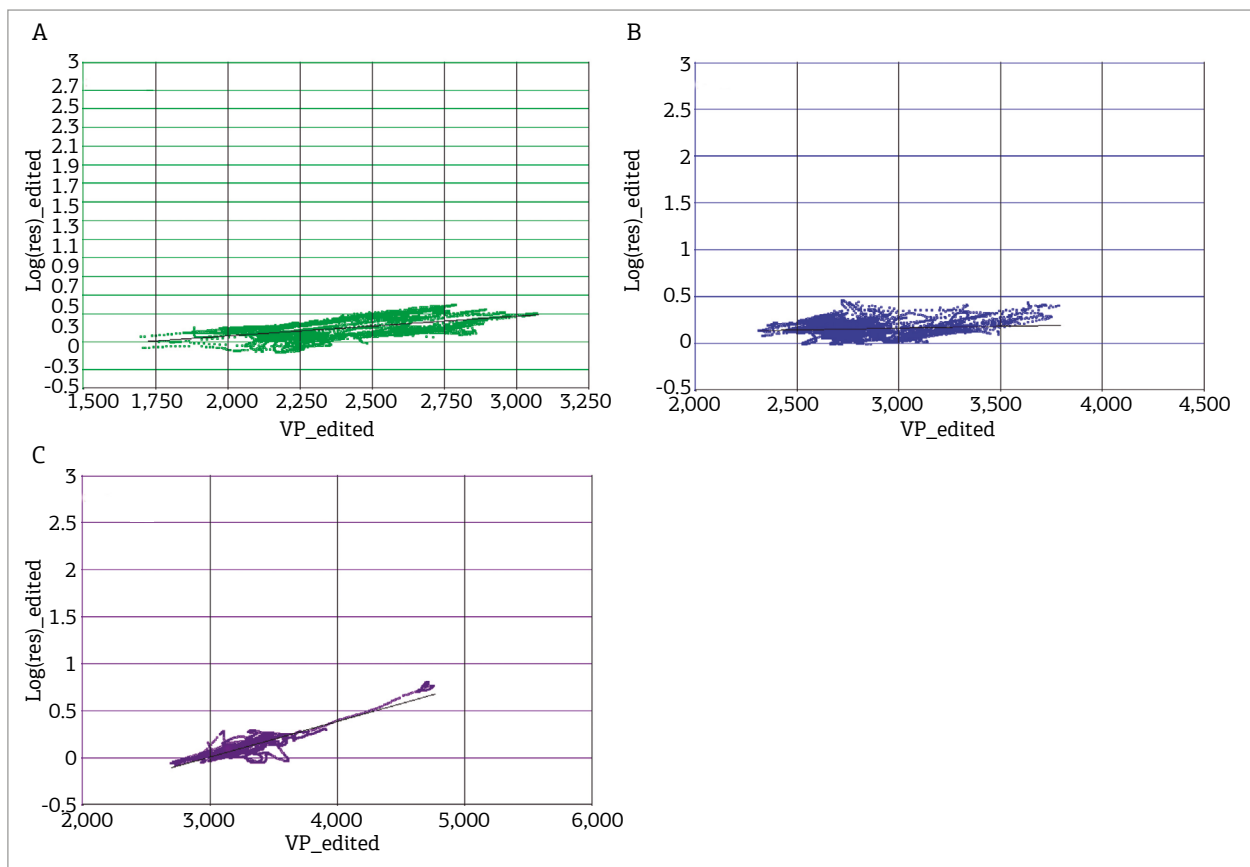Both anomalous and background relationships was used to convert the Vp cube into resistivity cube.

Figure 7. Relations between resistivity and *Vp* for all nine wells at three distinct depth intervals (Figure 6): (A) depth interval A; (B) depth interval B; (C) depth interval C.

Time to depth conversion

There are several methods for the time-depth (T–D) conversion. However, one can distinguish two main categories (Etris *et al.* 2001):

- Direct conversion;
- Velocity modeling.

We have followed the second option, by building an interval velocity model based on the well-log ties curves. Those were smoothed and interpolated along the studied area using the Horizon Cube. For the salt and subsalt sequences, we have applied, respectively, a constant 4,550 m/s interval velocity, and a velocity trend based on the studies of Bulhões *et al.* (2015).

The T–D conversion was made following two main steps, First of all, we did it only at seismic sections crossing the wells as a QC. Depth converted horizons were checked against the position of their correspondent stratigraphic marker at the wells. The final interval velocity model is shown in Figure 8.

In the second step, we used the 3D interval velocity model to convert to depth all the available property cubes: ρh, ρv , Vp, porosity and acoustic impedance and also the main stratigraphic horizons.

RESISTIVITY CUBES

To compute the ρh cube from the Vp cube, we developed a second algorithm (Algorithm 2). The input is the

---

input: V_p, φ and AI cubes
output: Resistivity of Marlim reservoirs

1 initialization;
2 **if** $AI \leq 5,700$ **then**
3   **if** $0.26 \leq \varphi \leq 0.32$ **then** $\rho_{hmarlim} = log_{10}(70)$;
4   **else** $\rho_{hmarlim} = \rho_{h200-2900m}$;
5 **end**
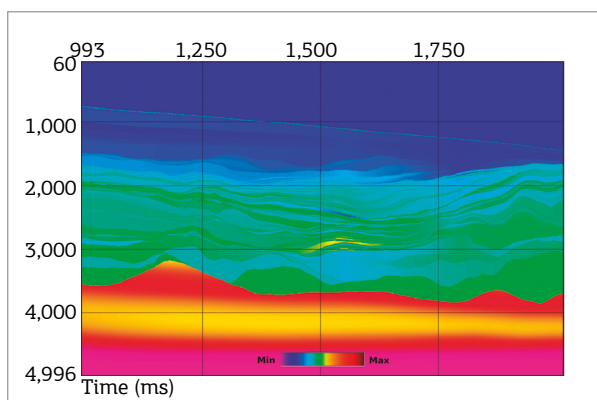
Algorithm 1. Marlim reservoir resistivities.

Figure 8. Interval Velocity, used in the time to depth conversion, extracted at Inline 327.

Vp, porosity and acoustic impedance cubes, but also some of the stratigraphic horizons.

Algorithm 2 implements both the background resistivities and incorporate algorithm 1 to distinguish between the reservoir and non-reservoir facies. We settled a stratigraphic window between the Top of Oligocene and BlueMark horizons (depth interval between 2,000–2,900m). BlueMark, a maximum flood surface of the Eo-Oligocene, is considered the base of the turbiditic reservoirs (Gamboa *et al.* 1986).

We used an anisotropic ratio ($\rho v / \rho h$) = 2.5 to calculate Marlim–R3D vertical resistivity cube from the horizontal resistivity cube (Park *et al.* 2015). That ratio was applied to the whole sedimentary section, except for the salt bodies that were handled as isotropic layers.

QUALITY CONTROL

To perform the quality control (QC) of the converted resistivity cube, we crossplot the recovered values against the measured resistivity in wells. Then we find a linear relationship by least-squares fitting, which fits both data to a specific correlation coefficient. That coefficient stands between 0 and 1 (0 to 100%).

For the sake of brevity, we show in Figure 9 the results for only one well: PS-W-01, which correlation coefficient is 0.95, *i.e.*, a 95% agreement between the modeled and measured resistivity was obtained.

As can be seen in Figure 9, the resistive turbidite sandstones that form the reservoir of the Marlim Field are properly outlined at depth, with top and base coinciding with the well information.

Figure 10 shows the vertical resistivity extracted along Top of Marlim horizon slice. The Marlim reservoir facies emerges as a high resistivity body embedded in a low-resistivity

---

input: V_p, φ, AI cubes and horizons in depth domain
output: Marlim R$_3$D horizontal resistivity cube

1 initialization;
2 if $depth \leq 2,000 \ m$ **then**
3   $\rho_h = \rho_{h600-2,000\ m} = -0.263 + 0.000166 V_p$;
4   **if** $2,000 \leq depth \leq 2,900$ **then**
    $\rho_h = \rho_{h2,000-2,900\ m} = -0.0683 + 0.000002798 V_p$;
5   **if** *Top of Marlim* $< depth <$ *Blue Mark* **then** execute algorithm 1;
    // distinguish between reservoir and non-reservoir resistivities
6   **if** *Top of Salt* $< depth <$ *Base of Salt* **then** $\rho_h = log_{10}(1,000)$;
    // Salt resistivity
7   **if** $depth \geq 2,900$ **then** $\rho_h = \rho_h > 2900 = -0.09 + 0.00037 V_p$

Algorithm 2. Calculation of the horizontal resistivity in the depth domain. Topof Marlim, Blue Mark, Top of Salt and Base of Salt are stratigraphic horizons.
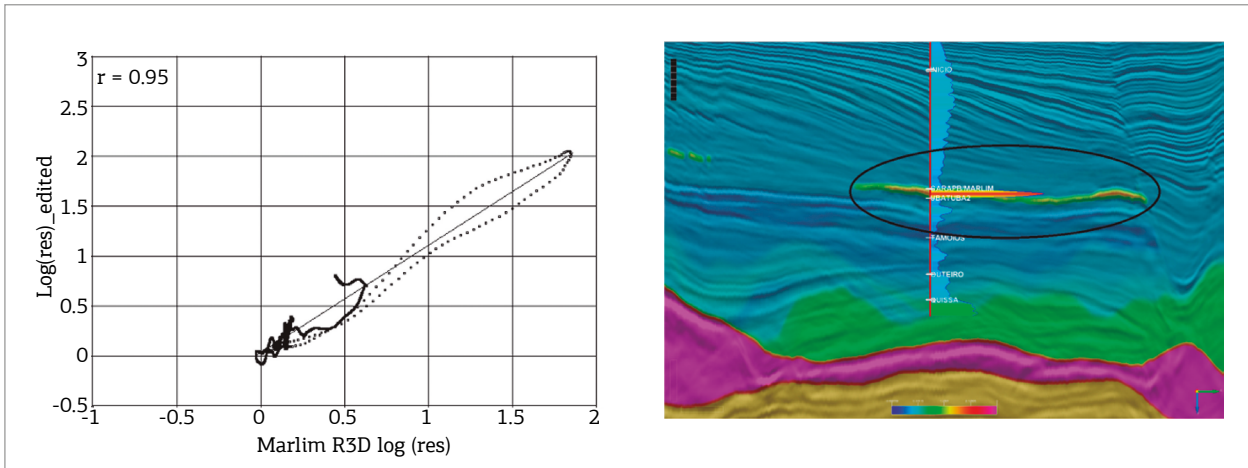

Figure 9. Right panel: crossplot between recovered ρh *versus* measured resistivity (ILD log) at PS-W-01 well. Left panel: comparison between the recovered ρh along an arbitrary section and the measured resistivity log at PS-W-01 well.
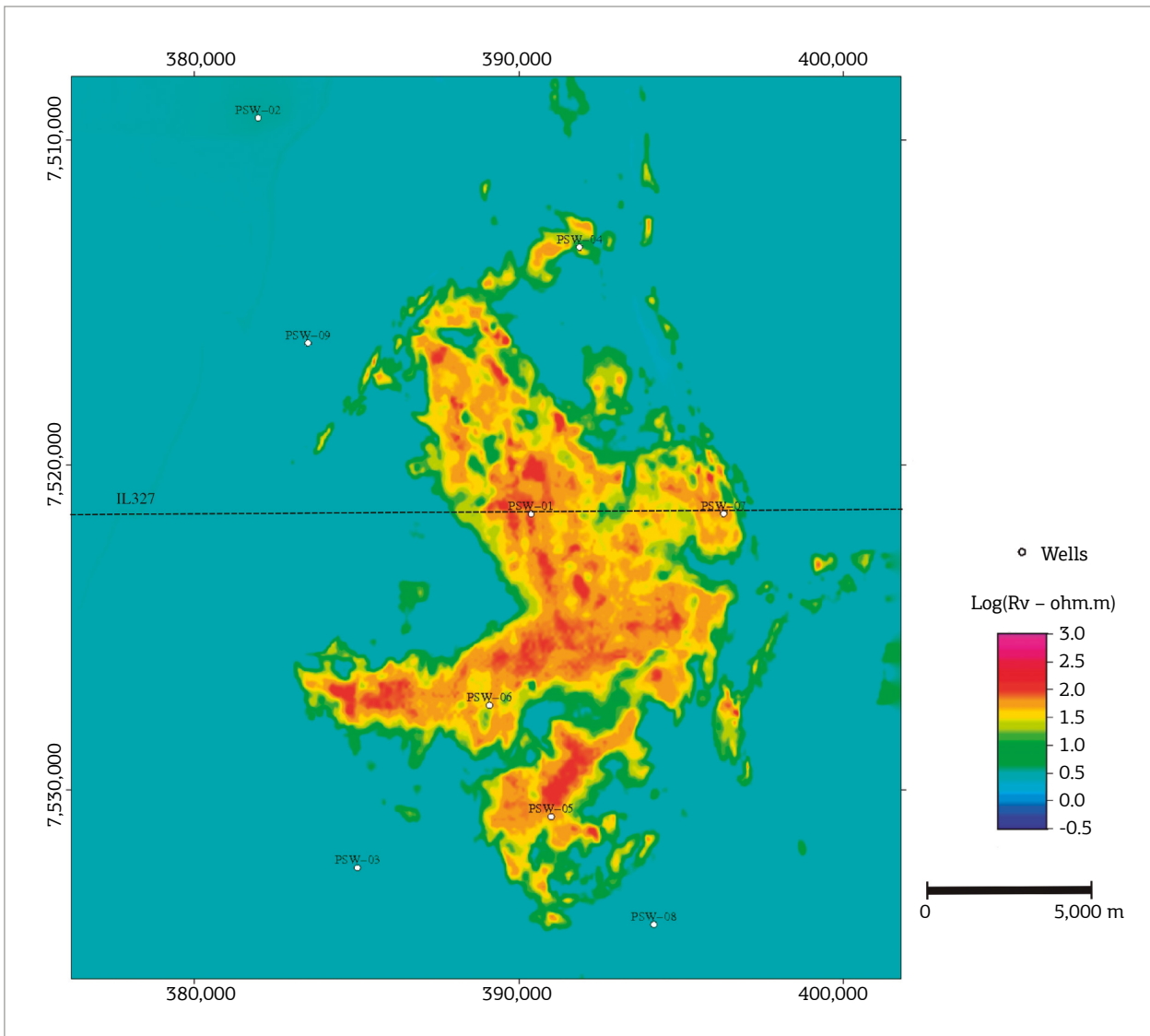

Figure 10. Map of the vertical resistivity distribution along a horizon at the top of Marlim reservoir. PSW-01 to PSW-09 are the available wells. The Marlim turbidites (clean sandstones) are clearly highlighted as high-resistivity bodies. Shale and shaly sand (non-reservoir) facies show lower ressitivity values.

background. Rather than a single resistivity body, as commonly pictured in most of the available resistivity models, including the SEAM-Phase I model, Marlim R3D exhibits a complex resistivity pattern. That is in agreement with the expected geological complexity of the turbidite bodies.

CONCLUSIONS

We present Marlim R3D, a realistic geoelectric model for CSEM simulations. The Marlim R3D aims to be a benchmark model for studies of turbiditic reservoirs.

The Marlim R3D model comprises a data set consisting of ρh and ρv cubes in SEG–Y format, the six stratigraphic horizons, and Vp, ρh and ρv , well-logs extracted from Marlim R3D in the position of nine wells. These well-logs aim to serve as a quality control of modeling and inversions studies using Marlim R3D.

These cubes are being made freely available to the general public on the Zenodo.

The cube is rendered in SGY format with data distributed along 75 × 25 × 5 m cells. We are currently developing a detailed 3D CSEM finite–difference forward study

to generate an official CSEM dataset for Marlim R3D. The full dataset will be soon delivered to general public at the Zenodo platform.

Although primarily conceived to be a CSEM reference model, Marlim R3D can also be used to simulate responses to any electromagnetic method such as marine magnetotellurics, surface-to-borehole EM, or even cross-well-EM studies.

ACKNOWLEGMENTS

REFERENCES

Bruhn C.H.L., Gomes J.A.T., Del Lucchese Jr.C., Johann P.R.S. 2003. Campos basin: Reservoir characterization and management-historical overview and future challenges. *In:* Offshore Technology Conference. Rio de Janeiro, p. 14

Bulhões F.C., Formento C.D.R., Lyrio J.C.O., Amorim G.A., Ferreira G.D., Pereira E.S., Castro R.F. 2015. Geostatistical 3d density modeling: Integrating seismic velocity and well logs. *In:* 14th International Congress of the Brazilian Geophysical Society & EXPOGEF. Rio de Janeiro, Brazilian Geophysical Society, p. 272-277.

Carcione J.M., Ursin B., Nordskag J.I. 2007. Cross-property relations be- tween electrical conductivity and the seismic velocity of rocks. *Geophysics*, **72**(5):E193-E204.

Carvalho B.R. & Menezes P.T.L. 2017. Marlim R3D - A Realistic Model For Mcsem Simulation. *Zenodo,* https://doi.org/10.5281/zenodo.400233.

Constable S. & Cox C.S. 1996. Marine controlled-source electromagnetic sounding: 2. the Pegasus experiment. *Journal of Geophysical Research,* **101**(B3):5519-5530.

Constable S. & Srnka L.J. 2007. An introduction to marine controlled-source electromagnetic methods for hydrocarbon exploration. *Geophysics,* **72**(2):WA3-WA12.

Edwards N. 2005. Marine controlled source electromagnetics: Principles, methodologies, future commercial applications. *Surveys in Geophysics,* **26**(6):675-700.

Etris E.L., Crabtree N.J., Dewar J. 2001. True depth con- version: More than a pretty picture. *Canadian Society of Exploration Geophysicists,* **26**(9):11-22.

Evans R.L., Sinha M.C., Constable S.C., Unsworth M.J. 1994. On the electrical nature of the axial melt zone at 13° N on the East Pacific Rise. *Journal of Geophysical Research,* **99**(B1):577-588.

Faust L.Y. 1953. A velocity function including lithologic variation. *Geophysics,* **18**(2):271-288.

Fehler M. 2009. SEAM phase I progress report: "classic" data sets. *The Leading Edge,* **28**(10):1178-1181.

Gamboa L., Esteves F., Shimabukuro S., Carminatti M., Peres W., Souza Cruz C. 1986. Evidˆencias de varia˛cˉoes de nivel do mar durante o oligoceno e suas implica˛cˉoes faciol´ogicas. *In:* SBG, Congresso Brasileiro de Geologia, p. 8-22.

Gomez C.T., Dvorkin J., Vanorio T. 2010. Laboratory measurements of porosity, permeability, resistivity, and velocity on Fontainebleau sandstones. *Geophysics,* **75**(6):E191-E204.

Groot P., Huck A., Bruin G., Hemstra N., Bedford J. 2010. The horizon cube: A step change in seismic interpretation! *The Leading Edge,* **29**(9):1048-1055.

Guardado L.R., Spadini A.R., Brandˉao J.S.L., Mello M.R. 2000. Petroleum system of the Campos Basin, Brazil. *American As- sociation of Petroleum Geologists,* 317-324.

Hashin Z. & Shtrikman S. 1962. A variational approach to the theory of the effective magnetic permeability of multiphase materials. *Journal of Applied Physics,* **33**:3125-3131.

Hermance J.F. 1979. The electrical conductivity of materials containing partial melt: A simple model from Archie's law. *Geophysical Research Letters,* **6**(7):613-616.

Johann P., Sansonowski R., Oliveira R., Bampi D. 2009. 4D seismic in a heavy-oil, turbidite reservoir offshore Brazil. *The Leading Edge*, **28**(6):718-729.

Leyden R., Asmus H., Zembruscki S., Bryan G. 1976. South Atlantic diapiric structures. *AAPG Bulletin*, **60**(2):196-212.

MacGregor L. & Tomlinson J. 2014. Marine controlled-source electromagnetic methods in the hydrocarbon industry: A tutorial on method and practice. *Interpretation*, **2**(3):SH13-SH32.

Mohriak W.U., Macedo J.M., Castellani R.T. 1996. Salt tectonics and structural styles in the deep-water province of the Cabo Frio region, Rio de Janeiro, Brazil. *The American Association of Petroleum Geologists Memoir* .

Mukerji T., Mavko G., Gomez C. 2009. Cross-property rock physics relations for estimating low-frequency seismic impedance trends from electromagnetic resistivity data. *The Leading Edge*, **28**(1):94-97.

Nascimento T.M., Menezes P.T.L., Braga I.L. 2014. High-resolution acoustic impedance inversion to characterize turbidites at Marlim Field, Campos Basin, Brazil. *Interpretation*, **2**(3):T143-T153.

Park J., Viken I., Menezes P.T.L., Filho C.E.B.L., Dabbadia M.R.A. 2015. Feasibility of borehole-surface EM for CO2 injection monitoring with a synthetic-field case. *In:* SEG Technical Program Expanded Abstracts. *Society of Exploration Geophysicists*, p. 1033-1038.

Qayyum F. & Smith D. 2014. Integrated sequence stratigraphy using trend logs and densely mapped seismic data. *First Break*, **32**(12):75-84.

Schön J.H. 2015. *Physical properties of rocks: Fundamentals and principles of petrophysics*. volume 65, Elsevier, 497p.

Tseng H.W., Stalnaker J., MacGregor L.M., Ackermann R.V. 2015. Multi-dimensional analyses of the SEAM controlled source electromagnetic data – the story of a blind test of interpretation workflows. *Geophysical Prospecting*, **63**(6): 1383-1402.

Werthmüller D., Ziolkowski A., Wright D. 2013. Background resistivity model from seismic velocities. *Geophysics*, **78**(4):E213-E223.

White R.E. & Simm R. 2003. Tutorial: Good practice in well ties. *First Break*, **21**.

Zerilli A., Buonora M.P., Menezes P.T.L., Labruzzo T., Marçal A.J., Crepaldi J.L.S. 2016. Broadband marine controlled-source electromagnetic for subsalt and around salt exploration. *Interpretation*, **4**(4):T521-T531.

Available at www.sbgeo.org.br